Langmuir

Article

pubs.acs.org/Langmuir

Understanding Surfactant/Graphene Interactions Using a Graphene Field Effect Transistor: Relating Molecular Structure to Hysteresis and Carrier Mobility

Chih-Jen Shih, Geraldine L. C. Paulus, Qing Hua Wang, Zhong Jin, Daniel Blankschtein, and Michael S. Strano*

Department of Chemical Engineering, Massachusetts Institute of Technology, Cambridge, Massachusetts 02139, United States

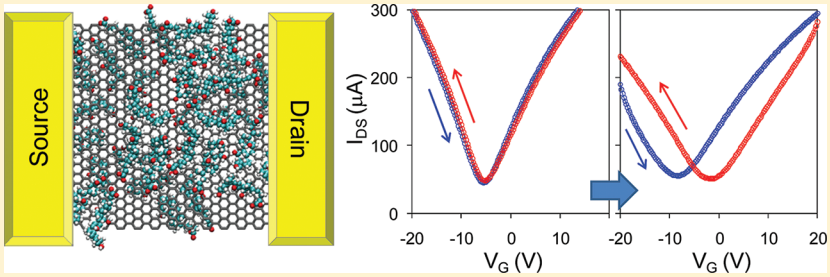

ABSTRACT: Manipulation of transport hysteresis on graphene transistors and understanding electron transfer between graphene and polar/ionic adsorbates are important for the development of graphene-based sensor devices and nonvolatile memory electronics. We have investigated the effects of commonly used surfactants for graphene dispersion in aqueous solution on transport characteristics of graphene transistors. The adsorbates are found to transfer electrons to graphene, scatter carrier transport, and induce additional electron−hole puddles when the graphene is on an SiO_2 substrate. We relate the change in transport characteristics to specific chemical properties of a series of anionic, cationic, and neutral surfactants using a modification of a self-consistent transport theory developed for graphene. To understand the effects of surfactant adsorbates trapped on either side of the graphene, suspended devices were fabricated. Strong hysteresis is observed only when both sides of the graphene were exposed to the surfactants, attributable to their function as charge traps. This work is the first to demonstrate the control of hysteresis, allowing us to eliminate it for sensor and device applications or to enhance it to potentially enable nonvolatile memory applications.

INTRODUCTION

Graphene, with atomic sheets consisting of fewer than 10 stacked layers of sp^2-hybridized carbon lattice,[1] has emerged as a promising candidate material for high-speed nanoelectronics due to its outstanding electronic properties.[2−4] Recent progress in tuning the bandgap and resistivity in AB-stacked bilayer[2,3,5] and trilayer[4] graphene have expanded our ability to control the properties of graphene for next-generation optoelectronic and microprocessor applications. These materials, nevertheless, require new synthesis methods for effective control over the number of AB-stacked layers using graphite exfoliation and processing. The conventional approach of micromechanically cleaved (Scotch tape) mono- and few-layer graphene[6] from graphite lacks an efficient mechanism for scalable manufacturing. Progress has been made on growth of large-area monolayer graphene using chemical vapor deposition (CVD) on metal catalysts and transfer to various substrates.[7−9] However, for bi- or trilayer applications, CVD graphene films tend to be turbostratic, where slight deviations from the AB stacking destroy the unique electronic structures of bilayer and trilayer graphene.[10,11] Exfoliation of pristine graphite into a liquid phase[12−14] is easily scalable and allows for more precise chemical modification in solution.[15,16] Very recently, our group has demonstrated a novel method to produce AB-stacked bilayer- and trilayer- enriched graphene dispersions in a sodium cholate (SC) aqueous solution using stage-controlled graphite intercalation compounds.[17] This approach enables the only viable route at this time to produce AB-stacked bi- and trilayer graphene on arbitrary substrates on a large scale, and the measured mobility values are the highest for any solution dispersed material to date.[17] However, compared to the "Scotch tape" devices, the transport characteristics are inferior in several respects.[17] Hysteresis and mobility loss are two properties investigated in the present work, with the hypothesis that surfactants commonly used to disperse pristine graphene are responsible for these effects.[17] In this work, we systematically investigate representative anionic, cationic, and neutral surfactants and their influence on carrier transport in graphene transistors.

An important feature of graphene electronic structure is its low density of states near the Dirac point at which the conduction and valence bands meet, such that the electronic

Received: February 29, 2012
Revised: May 10, 2012
Published: May 15, 2012

   dx.doi.org/10.1021/la3008816 | Langmuir 2012, 28, 8579−8586

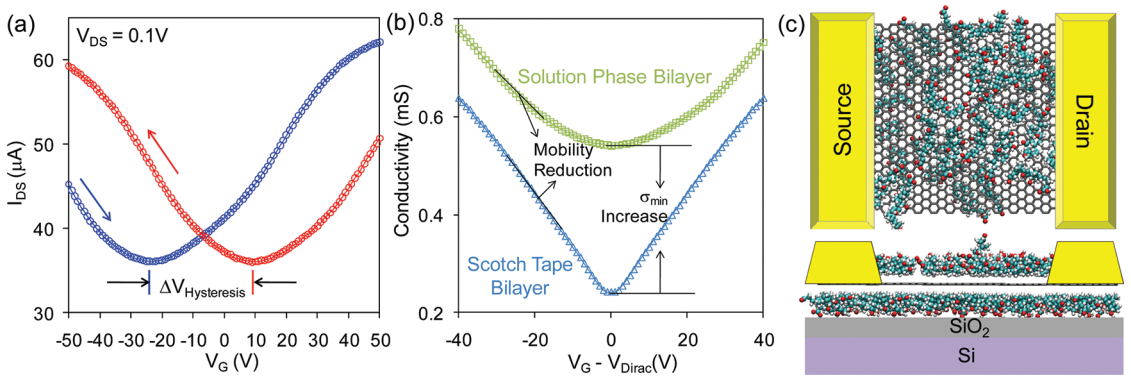

Figure 1. Effects of adsorbed sodium cholate (SC) molecules on solution-phase bilayer graphene transistors. (a) I_{DS}–V_G curves of the graphene device using a bilayer graphene flake dispersed in SC aqueous solution. The arrows indicate the direction of the gate voltage sweep. (b) Normalized 2D conductivity vs gate voltage (V_G–V_{Dirac}) of a Scotch tape exfoliated (blue) and a solution phase (green) bilayer graphene device showing the mobility reduction and the minimum conductivity (σ_{min}) increase. (c) Top-view (top) and side-view (bottom) schematics of a solution-phase graphene transistor with SC coated on both sides.

properties are very sensitive to the surroundings. The formation of electron–hole puddles[18] near the charged impurity centers on SiO_2 substrate[19] has been proven to scatter carrier transport. Therefore, recent experimental efforts have demonstrated that the transport characteristics of graphene transistors can be greatly improved using the hydrophobic,[20,21] self-assembled monolayers (SAM),[22,23] crystalline hexagonal boron nitride (hBN),[24] and suspended substrates.[25] On the other hand, the effects of adsorbates on graphene transistors have been extensively studied to control transport characteristics for graphene sensor applications. N-type adsorbates, e.g., NH_3 vapor,[26] CO vapor,[26] 1,5-naphthalenediamine vapor,[27] liquid poly(ethylene imine) (PEI),[28] 1,5-naphthalenediamine ($NaNH_2$),[27] 9,10-dimethylanthracene (An-CH_3),[27] and aluminum thin film,[29,30] donate additional electrons to graphene. On the other hand, P-type doping has been observed in graphene transistors exposed in dilute H_2O and NO_2 vapors,[26] O_2 gas,[31,32] tetrasodium 1,3,6,8-pyrenetrtrasulfonic acid (TPA) vapor,[27] tetrafluoro-tetracyanoquinodimethane (F4-TCNQ),[33] 9,10-dibromoanthracene (An-Br),[27] tetrasodium 1,3,6,8-pyrenetetrasulfonic acid (TPA),[27] and diazonium salt solutions.[28] There are some reports indicating that transport characteristics can be changed by the solution pH.[34,35] However, there is a dearth of literature on commonly used surfactants for graphene dispersion and their potential influence on carrier transport. Also unknown is how the specific chemical structure of the surfactant alters electronic and transport properties.

In our previous study,[17] transistors produced using solution-phase bilayer graphene flakes have shown an ambipolar behavior, and the calculated mobility is about 400 $cm^2\ V^{-1}\ s^{-1}$. In addition, by applying top-gate engineering, we have shown that its Dirac point moves along the diagonal, and the 2D resistivities reach a maximum at the upper-left and lower-right corners in the two-dimensional contour plot of 2D resistivities versus top-gate and bottom-gate voltages.[17] With this work, the high mobility and the vertical electric field induced characteristics were demonstrated in solution phase graphene for the first time.[17]

The purpose of this paper is to understand the effects of anionic, cationic, and neutral surfactants on carrier transport in graphene transistors. The dipole nature of surfactants and their electronic interaction with graphene result in peculiar transport phenomena compared to well-studied dopants.[26−32] To rationalize these interactions, we use a modified self-consistent transport theory[19] that considers the effects of specific dopants. Interestingly, we find an enhancement of hysteresis when surfactants are allowed to adsorb to both sides of the graphene, as in the case of suspended devices. Using this approach, for the first time, we report a new method to eliminate and further control the electronic hysteresis in graphene transistors. These findings facilitate understanding the response of carrier transport in graphene to dipole adsorbates, and developing novel graphene devices for biosensing and nonvolatile memory applications.

RESULTS AND DISCUSSION

Compared to bilayer graphene devices prepared from Scotch tape exfoliation, we notice two distinct differences in the transfer characteristics of those fabricated from surfactant dispersed solution, as shown in Figure 1, panels a and b. All of the source-drain current (I_{DS}) vs gate voltage (V_G) curves were measured at ambient conditions, and the devices were fabricated on 100 nm SiO_2/p-doped Si substrates. First, a pronounced hysteresis is exhibited by sweeping the gate voltage from −50 to +50 V and back to −50 V (see Figure 1a). For each curve, we carried out voltage sweeping multiple (∼10) times until we obtained stable characteristics and saturated hysteresis, such that $V_{Hysteresis}$ is independent of sweeping speed and voltage range.[22,36] When the gate starts at negative voltage, charges (holes) in graphene are gradually injected into the traps at bulk gate dielectrics and the graphene–dielectric interface such that graphene senses a more positive potential than that due to the gate voltage (and vice versa).[22,36] The difference between the Dirac points, V_{Dirac}, (the gate voltage corresponding to the minimum conductivity, σ_{min}, of the I_{DS}–V_G curve) measured using positive and negative voltage sweeps, $\Delta V_{Hysteresis}$, can be used to estimate the density of traps, n_{trap}, as follows:

$$n_{trap} = \frac{\Delta V_{Hysteresis} C_G}{e} \quad (1)$$

where C_G is the gate capacitance and e is the unit charge. The calculated n_{trap} value corresponding to the $\Delta V_{Hysteresis}$ in Figure 1a is 5.8 × 10^{12} cm^{-2}, which is anomalously 1 order of magnitude higher than the reported density of traps in bulk SiO_2, n_{it} (∼5 × 10^{11} cm^{-2}).[36,37] Second, compared to the Scotch tape bilayer device, a ∼60% reduction of hole mobility,

dx.doi.org/10.1021/la3008816 | Langmuir 2012, 28, 8579–8586

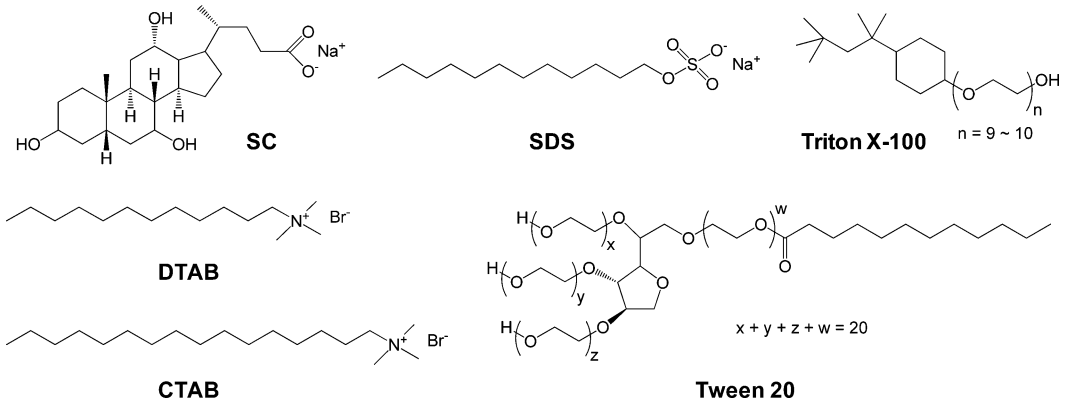

Figure 2. Chemical structures of the surfactants considered in this work.

Table 1. Surfactant Type, Critical Micelle Concentration (CMC), Concentration, Charge, and Its Counterion for the Surfactants Considered in This Study

	surfactant	CMC (mM)	MW	CMC (wt%)	concentration (wt%)	charge	counterion
anionic	SC	12	431	0.52%	2%	−1	Na^+
	SDS	8.7	288	0.25%	1%	−1	Na^+
nonionic	Triton X-100	0.55	625	0.034%	0.1%	0	
	Tween 20	0.06	1228	0.0074%	0.025%	0	
cationic	CTAB	1	364	0.036%	0.12%	+1	Br^-
	DTAB	14.1	308	0.43%	1.3%	+1	Br^-

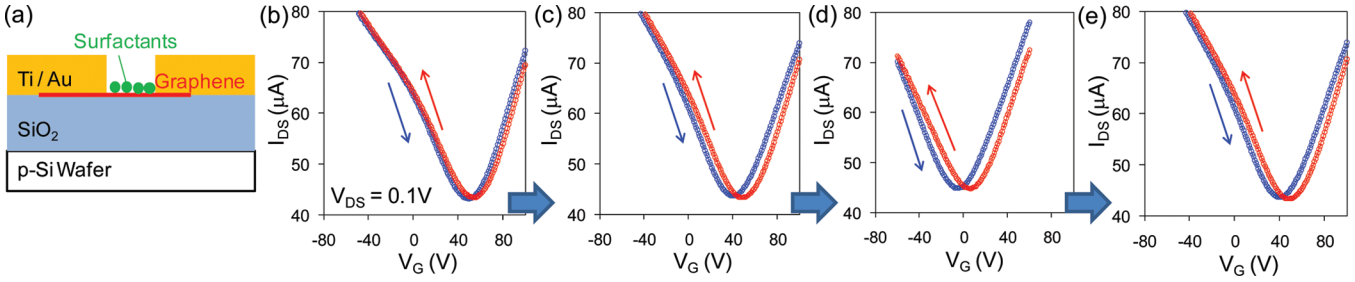

Figure 3. (a) Schematic diagram of a graphene device with surfactants adsorbed on the top side, (b–e) The sequential experiments and $I_{DS}-V_{GS}$ curves showing the effects of sodium cholate (SC) adsorbing on top of a representative graphene device (trilayer): (b) the as-prepared device, (c) after dipping into pure water and blowing dry, (d) after dipping into SC aqueous solution and blowing dry, and (e) after final water rinsing and blowing dry.

μ, and ~65% increase of minimum conductivity, σ_{min}, are observed (see Figure 1b). Since the Raman spectra of these solution phase graphene flakes lack an appreciable D peak,[17] we believe that the lattice structure of our solution phase graphene was preserved during the intercalation, expansion, and dispersion processes.[17] Therefore, the main factor that influences the transport characteristics is hypothesized to be trapped surfactant adsorbates. Top-view and side-view schematic diagrams of a solution-phase graphene transistor coated with sodium cholate (SC) are shown in Figure 1c. The observed change of transport characteristics, however, is not consistent with those reported using standard n- or p-type adsorbants on graphene transistors.[26−32] According to other reports in the literature, the transfer characteristics of a graphene transistor after adsorbate doping exhibit (i) asymmetric electron−hole conduction[28] (i.e., only one side (electron or hole) of mobility is reduced) and (ii) reduction (not increase) of σ_{min}.[28,30]

In order to understand the effects of surfactant adsorbates on the transfer characteristics of graphene transistors, graphene devices were fabricated using the Scotch tape exfoliation process to isolate graphene flakes on 300 nm SiO_2/p-doped Si substrate. Before graphene exfoliation, the SiO_2 substrates were cleaned with copious amounts of acetone, isopropanol (IPA), and DI water. Following that, they were exposed to O_2 plasma at 200 W for 3 min. The layer number of the graphene flakes was identified based on their contrast ratio in optical microscopy and on their characteristic Raman spectra. Conventional ultraviolet lithography was utilized to pattern the source/drain contacts onto the flakes. The electrodes were then prepared by electron beam deposition of 25/75 nm thick Ti/Au layers sequentially under high vacuum. Finally, the devices were soaked in acetone overnight to lift off the remaining photoresist. Before electronic characterization, each device was rinsed with IPA and dried with a nitrogen gun. All measurements were carried out at ambient conditions. The anionic, cationic, and nonionic surfactants considered here were: sodium cholate (SC), sodium dodecylsulfate (SDS), dodecyltrimethyl ammoniumbromide (DTAB), cetyltrimethyl ammoniumbromide (CTAB), Triton X-100, and Tween 20. All of these surfactants are known to be effective in dispersing graphene in aqueous media.[13,38,39] The chemical structures of

dx.doi.org/10.1021/la3008816 | Langmuir 2012, 28, 8579−8586

these surfactants are shown in Figure 2. For all surfactants, the surfactant type, critical micelle concentration (CMC), concentration, surfactant charge, and counterion are listed in Table 1.

First, we study the effects of the surfactant adsorbates on the top side of graphene open to the surroundings but otherwise on a SiO_2 surface. The schematic diagram is shown in Figure 3a. Several monolayer, bilayer, and trilayer devices were fabricated and characterized before surfactant adsorption. A series of experiments and measurements were then carried out using these devices sequentially. The change of transport characteristics for a representative device (trilayer) is shown in Figure 3, panels b–e. Figure 3b shows the I_{DS}–V_G curves of the as-prepared device, and the arrows indicate the direction of the gate voltage sweep. The V_{Dirac} is located at 50 V, and the $\Delta V_{Hysteresis}$ is 5 V. The positive V_{Dirac} is believed to be mainly caused by the electron–hole puddles on the SiO_2 surface[19] and other p-type adsorbates from the surroundings (e.g., O_2[31,32] and H_2O[26]). The calculated n_{trap} corresponding to the $\Delta V_{Hysteresis}$ is 3.6×10^{11} cm^{-2}. This value is of the same order as the reported density of traps in bulk SiO_2, n_{it}. The transport characteristics are very stable in air, and the I_{DS}–V_G curves remain almost the same after dipping the device into DI water and blowing dry with nitrogen (Figure 3c). Since the sensitivity of graphene to water has been well studied,[26] it appears that the concentration of H_2O adsorbates on the graphene surface is saturated before immersion. The surfactant adsorbates were introduced by dipping the device into a SC aqueous solution (5 min) and blowing dry. Figure 3d shows the I_{DS}–V_G curves of the surfactant adsorbed device. Compared to the as-prepared device, we found that (i) the V_{Dirac} shifts back to +5 V, (ii) there is an increase of σ_{min} and a reduction of carrier mobility, and (iii) $\Delta V_{Hysteresis}$ is increased to 9 V. The negative V_{Dirac} shift suggests that the SC adsorbates "n-dope" the graphene device. However, the electron–hole conduction is symmetric and both hole and electron mobilities are reduced. These observations are consistent with those found in our solution-phase devices, but it conflicts with those for standard n-type dopants,[26–32] as we indicated above. The final rinsing of the device with a large amount of water can remove the surfactant adsorbates on the graphene device so that the I_{DS}–V_G curves are restored, as shown in Figure 3e. These results (see Figure 3, panels b–e) indicate that the effects of surfactant adsorbates on the top side of graphene are pronounced but reversible. The intrinsic properties of graphene appear unchanged during these experiments. The change of transport characteristics can serve as a powerful tool to quantify the interactions between surfactant adsorbates and graphene.

The same experiments were performed on several mono-, bi-, and trilayer graphene devices with the six surfactants considered in this study. The V_{Dirac} change and the percentage change of the hole mobility and σ_{min} for each device before and surfactant adsorption are plotted in Figure 4a. The charges before and after water dipping are also shown for comparison. For some data points, we notice a significant spread in calculated properties. One reason for this may be uncontrolled crystallization or aggregation of the surfactants on the graphene surface during the drying process. However, since the changes of characteristics after water dipping alone are much smaller than this spread (see Figures 3c and 4a), it appears that the device-to-device variation itself is not responsible. Several important observations about the effects of surfactant adsorbates can be summarized as follows: (i) For all of the surfactants considered, the adsorbates reduce mobilities and

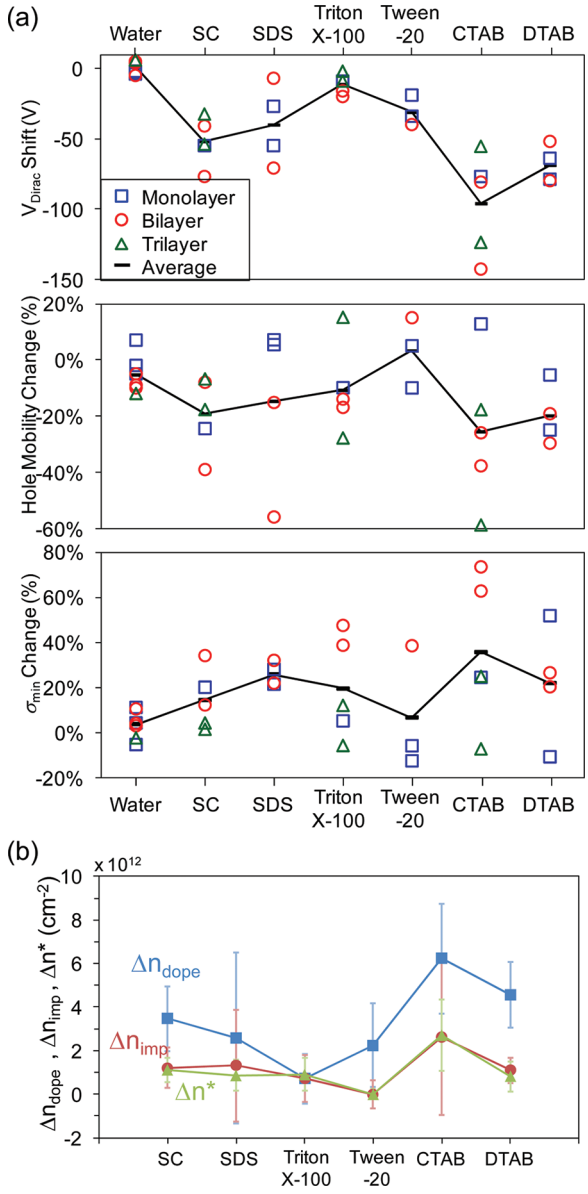

Figure 4. Quantitative analyses of the effects of surfactants adsorbing on the top side of graphene devices. (a) Shift of the Dirac point and the percentage change of hole mobility and minimum conductivity for various graphene devices (blue square, monolayer; red circle, bilayer; and green triangle, trilayer) with respect to different surfactants. (b) Calculated Δn_{dope}, Δn_{imp}, and Δn^* with respect to different surfactants.

increase σ_{min}. (ii) All of the six surfactants can be classified as n-dopants according to the standard interpretation used in the literature to date[26–32] since the V_{Dirac} changes are all negative. (iii) On average, we can rank the surfactant types according to the change of the transport characteristics as follows: cationic > anionic > nonionic surfactants. (iv) CTAB influences the transport characteristics more than DTAB.

To rationalize these observations, we use a modification of the self-consistent transport theory[19] advanced by Das Sarma et al., where an additional term is included to take into account the effects of the additional dopants. Specifically, the carrier transport in a graphene transistor considering the effects of the underlying SiO_2 and the adsorbates on top is given by

dx.doi.org/10.1021/la3008816 | Langmuir 2012, 28, 8579–8586

$$\sigma(n) = \frac{2e^2}{hn_{imp}G[r_s]}\sqrt{(n + \bar{n} + n_{dope})^2 + n^{*2}}$$

$$G[x] = x^2\left[\frac{\pi}{4} + 3x - \frac{3\pi x^2}{2} + \frac{x(3x^2 - 2)\arccos[1/x]}{\sqrt{x^2 - 1}}\right], \bar{n} = \frac{n_{imp}^2}{4n^*} \quad (2)$$

where σ is the conductance, h is the Planck constant, n is the carrier (electron or hole) density, n_{imp} is the concentration of charged impurities created near the graphene surfaces that scatter carrier transport, n_{dope} is the concentration of carriers doped due to the adsorbates, and n^* is the residual density of electron–hole puddles on SiO_2 surface that screen the electric potential from the bottom gate.[19] In eq 2, r_s is the dimensionless constant describing the coupling strength of the dielectrics to graphene, $r_s = 2e^2/h\varepsilon_0 v_F(\kappa_1 + \kappa_2)$,[40] where v_F is the Fermi velocity of graphene (1.1×10^6 m/s),[19,40] ε_0 is the vacuum permittivity, and κ_1 and κ_2 are the dielectric constants of SiO_2 (~3.9) and air (~1), respectively. Compared to the self-consistent transport theory[19] proposed by Adam et al.,[19] we introduce the n_{dope} term to describe the charge transfer between graphene and surfactant adsorbates. Using eq 2, the μ, V_{Dirac}, and σ_{min} can be expressed analytically as follows:

$$\mu = \frac{1}{e}\frac{d\sigma}{dn} = \frac{2e}{hn_{imp}G} \quad (3)$$

$$\sigma_{min} = \frac{2e^2}{hn_{imp}G}|n^*| \quad (4)$$

$$V_{Dirac} = -\frac{(n_{dope} + \bar{n})e}{C_G} \quad (5)$$

Note that eqs 3–5 suggest that (i) the reduction of mobility originates from the increase of n_{imp} on graphene surfaces, (ii) the positive n_{dope} (electrons) causes a negative shift of V_{Dirac}, and (iii) the increase of σ_{min} results from the increase of n^*. However, it is noteworthy that n^* is associated with the density of electron–hole puddles, which screen the electric potential of the bottom gate, at the graphene–SiO_2 interface.[19] The surfactant adsorbates are not able to penetrate this interface due to the strong interactions between graphene and the SiO_2 substrate. Using these equations, Δn_{imp}, Δn^*, and Δn_{dope}, which correspond to the change of n_{imp}, n^*, and n_{dope} due to the surfactant adsorbates, can be calculated analytically from the experimentally obtained μ, σ_{min}, and V_{Dirac}. It is noteworthy that although this model was derived for monolayer graphene devices,[19] the Δn_{imp}, Δn^*, and Δn_{dope} for bilayer and trilayer graphene devices were extracted using the same equations since the graphene layer dependence is weak (see Figure 4a). The calculated values with respect to the six surfactants considered are shown in Figure 4b.

For all the six surfactants considered, the concentrations of n_{imp}, n^*, and n_{dope} are increased due to the adsorbates. In other words, the surfactants scatter carrier transport, transfer electrons to graphene, and screen the effective electric potential from the bottom gate. On average, the surfactant adsorbates create 5×10^{11}~2×10^{12} cm^{-2} n_{imp} and n^*, and 1×10^{12}~6×10^{12} cm^{-2} electrons (n_{dope}) is doped to graphene. The trends for Δn_{imp}, Δn^*, and Δn_{dope} with respect to different surfactants are very similar. The theoretical picture behind these behaviors can be explained as follows. Surfactants are polar, amphiphilic compounds containing both hydrophobic tails and hydrophilic heads. Since the graphene surface is very hydrophobic, the hydrophobic tails of the surfactant adsorbates tend to stay close to the surface, while the hydrophilic heads prefer to remain hydrated and away from the graphene. The close distance (~3 Å) between the adsorbed surfactants and graphene causes a degree of electron transfer such that additional electrons are doped (n_{dope}) to graphene. Therefore, the surfactant adsorbates on graphene can be viewed as clusters of dipole units, which scatter the carrier transport (i.e., increase n_{imp}). In this respect, ionic surfactants possess stronger polarity than nonionic surfactants, and therefore, the change of the transport characteristics is more pronounced. CTAB is more polar than DTAB due to its longer hydrophobic tail. As a result, it affects the transport characteristics more significantly. These dipoles also interact with the electron–hole puddles on the SiO_2 substrate through graphene, since the graphene is too thin to screen their electric fields. Consequently, the density of the electron–hole puddles (n^*) is increased due to this electrostatic induction such that the effective electric potential from the bottom gate is reduced. On the other hand, the negative partial charges on the SiO_2 surface, which were generated during the O_2 plasma cleaning process, also alter the arrangement of the surfactants on the top side of graphene. The hydrophilic heads of cationic surfactants tend to stay closer to the graphene surface than those of anionic surfactants due to the electrostatic attraction from the SiO_2 substrate. As a result, the cationic surfactants considered are found to change transport characteristics more significantly than the anionic surfactants considered. The unusual changes of transport characteristics can be understood in terms of the strength of surfactant polarity and the interactions between the surfactant dipoles, graphene, and the underlying SiO_2.

The influence of the surfactant adsorbates on the electronic hysteresis was also investigated. Figure 5 shows the $\Delta V_{Hysteresis}$

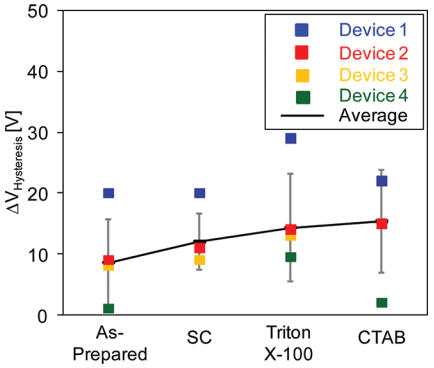

Figure 5. Measured $\Delta V_{Hysteresis}$ for four different devices with respect to different surfactants adsorbed on the top side of graphene.

for four devices before and after adsorption of three different surfactants. We found that the average n_{trap} corresponding to the $\Delta V_{Hysteresis}$ for as-prepared devices is about 7×10^{11} cm^{-2}, and a small, weak increase of n_{trap}, up to 1×10^{12} cm^{-2}, is exhibited when the surfactant adsorbates are on the top side of graphene (see Figures 3 and 5). Nevertheless, the surfactant dependence is weak, and although this value is higher than that of n_{it} (~5×10^{11} cm^{-2}), it is much lower than the one that we observed in our solution-phase graphene (~5×10^{12} cm^{-2}). As

dx.doi.org/10.1021/la3008816 | Langmuir 2012, 28, 8579–8586

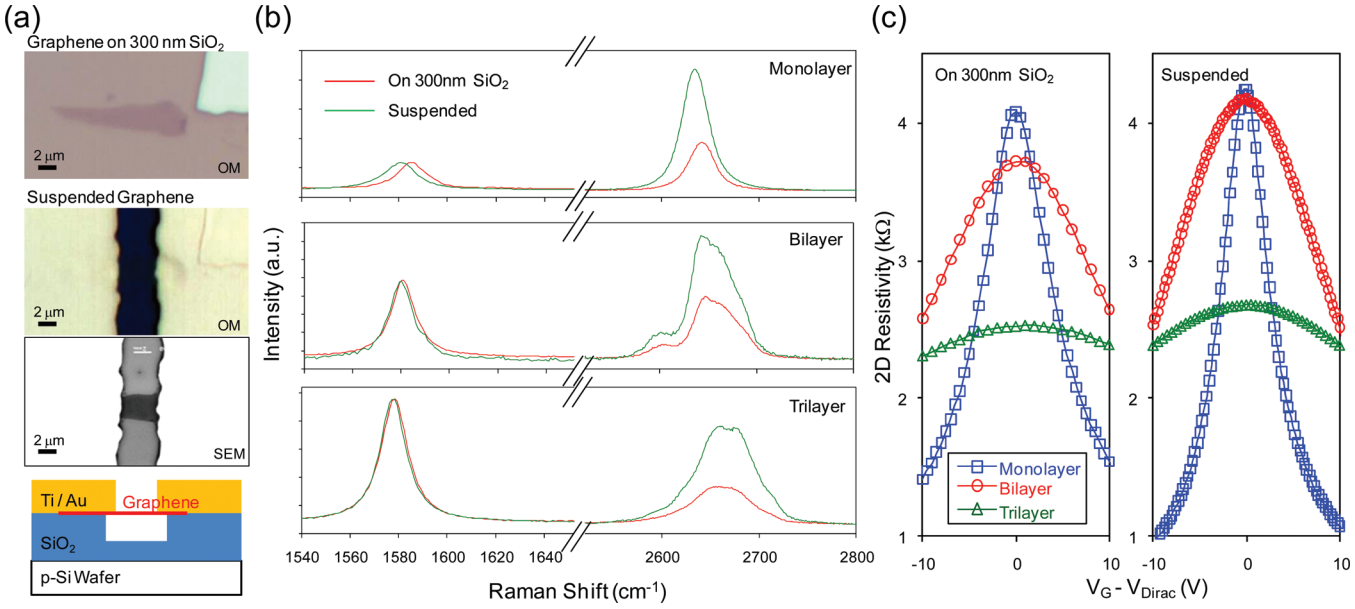

Figure 6. Fabrication and Characterization of suspended graphene transistor devices. (a) Top to bottom: Optical microscope (OM) image of an exfoliated graphene flake on 300 nm SiO_2, OM and SEM images of the suspended graphene flake held between two electrodes, and the side-view of the device schematic. (b) Raman spectra and (c) Normalized 2D resistivity vs gate voltage of monolayer, bilayer, and trilayer graphene on 300 nm SiO_2 and after suspension.

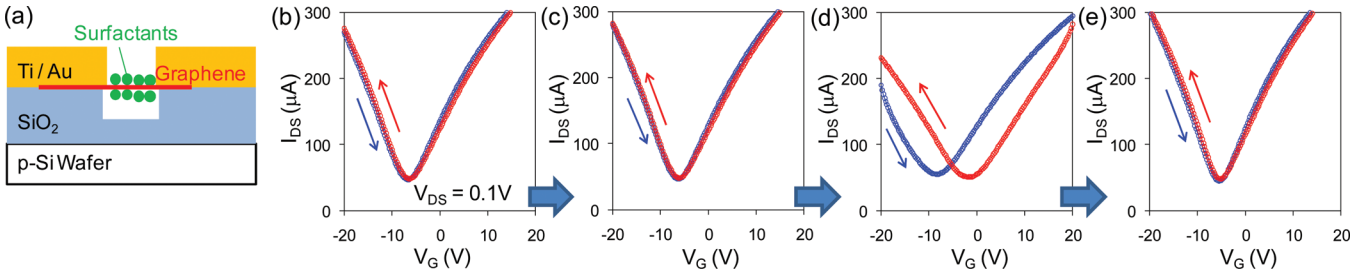

Figure 7. (a) Schematic diagram of a suspended graphene device with surfactants adsorbed on both sides. (b–e) The sequential experiments and I_{DS}–V_{GS} measurements showing the effects of sodium cholate (SC) on both sides of a suspended monolayer device: (b) the as-prepared device, (c) after dipping into pure water and blowing dry, (d) after dipping into SC aqueous solution and blowing dry, and (e) after final water rinsing and blowing dry.

we mentioned above, the n_{trap} is associated with the density of the traps at bulk gate dielectrics and the graphene–dielectric interface.[22,36] The small increase of n_{trap} most likely results from the electrostatic induction from the surfactant dipoles on the top of graphene, which is similar to the formation of Δn^*. However, we did not find an obvious surfactant-dependence in the series of experiments, and the anomalously high n_{trap} observed in our solution-phase graphene cannot be fully understood unless we fabricate a graphene device with surfactants on both sides of graphene.

In order to make the graphene-dielectric interface accessible to the surfactant adsorbates, suspended mono-, bi-, and trilayer devices were fabricated using the method proposed by Bolotin et al.[25] Briefly, the graphene devices on SiO_2 were immersed in 7:1 buffered oxide etch for 90 s, which etches approximately 50% of the SiO_2, including the area under the graphene,[41] as shown in Figure 6a. After suspension, the graphene flake is almost invisible under an optical microscope but still clear under SEM. The representative Raman spectra (using He–Ne laser at 633 nm) for mono-, bi-, and trilayer graphene before and after suspension are shown in Figure 6b. For the suspended monolayer graphene, the G peak (at 1580 cm^{-1}) is downshifted by 6 cm^{-1} compared to the one on the substrate because the effects of the SiO_2 substrate are removed.[42,43] As a result, the intensity ratio of the 2D (at 2633 cm^{-1}) and G peaks, I_{2D}/I_G, is also enhanced by a factor of 4 for the suspended monolayer.[38] The location of the G peak for the suspended bilayer and trilayer graphene does not shift obviously, but the I_{2D}/I_G is still enhanced about 2–3 times. This is because the effects of the substrate are reduced by the additional stacking layer(s), and the change of I_{2D}/I_G is much more sensitive to the carrier concentration than the G peak position near the Dirac point.[44] The obvious change of Raman spectra indicates that the suspended devices were fabricated successfully.[43] Figure 6c shows the representative 2D resistivities as a function of normalized gate voltage for mono-, bi-, and trilayer devices before and after suspension. All curves were measured at ambient conditions. The highest mobility at 25 °C for our suspended monolayer is 20 000 $cm^2\ V^{-1}\ s^{-1}$. The large mobility enhancement compared to the one on the SiO_2 surface (6000 $cm^2\ V^{-1}\ s^{-1}$) results from the substantial reduction of extrinsic scattering (n_{imp}).[25]

A series of experiments (see Figure 3) were carried out using the suspended devices to understand the effects of the

dx.doi.org/10.1021/la3008816 | Langmuir 2012, 28, 8579–8586

surfactant adsorbates on both sides of graphene. Figure 7a shows a schematic diagram of the device, and the change of transport characteristics for a representative device (monolayer) is exhibited in Figure 7, panels b–e. Figure 7b shows the $I_{DS}-V_G$ curves of the as-prepared device. The V_{Dirac} is located at −7 V, and the $\Delta V_{Hysteresis}$ is 0.5 V. Since the graphene is already suspended, the negative V_{Dirac} may result from the residuals generated during device fabrication. The calculated n_{trap} corresponding to the $\Delta V_{Hysteresis}$ is only 1.5×10^{10} cm^{-2}, which is several tens of times lower than that on SiO_2.[36] Again, the transport characteristics remain almost the same after dipping the device into DI water and blowing dry (Figure 7c). The hysteresis is introduced after dipping the device into SC aqueous solution and blowing dry, as shown in Figure 7d. It appears that the surfactant adsorbates at the graphene–dielectric interface create an increase in n_{trap}. Figure 7e indicates that final rinsing of the device with a large amount of water can restore the transport characteristics. The suspended architecture presented here not only demonstrates the highest quality of graphene device[25] but probably represents the simplest method to suppress hysteresis to a very high degree at ambient conditions compared to other methods.[21,23] Most importantly, it provides a reversible and controllable platform to create hysteresis artificially.

Several suspended mono-, bi-, and trilayer graphene devices were fabricated and tested with the six surfactants considered. The $\Delta V_{Hysteresis}$ values for each device before and after surfactant adsorption are plotted in Figure 8a. The average

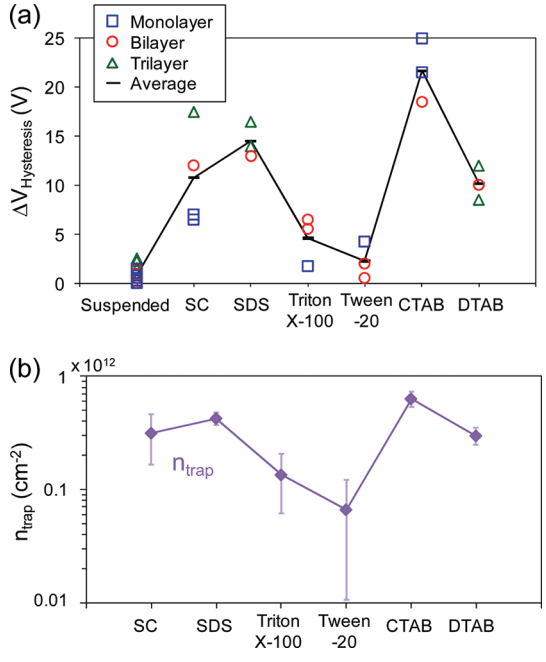

Figure 8. (a) Measured $\Delta V_{Hysteresis}$ and (b) calculated n_{charge} for various suspended devices with respect to different surfactants.

$\Delta V_{Hysteresis}$ for the suspended devices is only 0.8 V ($n_{trap} = 1.5 \times 10^{10}$ cm^{-2}), and the degree of hysteresis is also highly surfactant-dependent. Figure 8b shows the calculated n_{trap} using the six surfactants. For ionic and nonionic surfactant adsorbates, $(2–6) \times 10^{11}$ cm^{-2} and $0.(5–1) \times 10^{11}$ cm^{-2} traps are created, respectively. The surfactant dependence also suggests that the higher dipole strength of the surfactant can create more traps.[22,36] Accordingly, using the suspended device structure, the degree of hysteresis can be controlled by modulating the polarity of the surfactant adsorbates.

CONCLUSIONS

In summary, we investigated the effects of surfactant adsorbates on transport characteristics in graphene transistors. The adsorbates are found to transfer electrons to graphene, scatter carrier transport, and induce more electron–hole puddles on the SiO_2 substrate. Therefore, the surfactant-doped devices show negative V_{Dirac} shift, reduced mobility, and increased σ_{min}, which have never been reported. The mechanism behind the unusually observed behaviors can be rationalized using a new theoretical model based on the self-consistent transport theory.[19] Therefore, all of the changes of transport characteristics can be quantitatively analyzed using the extracted n_{dope}, n_{imp}, and n^* values. We found that the change of transport characteristics is surfactant-dependent, and results from the dipolar nature of the surfactants and the interactions between surfactant adsorbates, graphene, and underlying SiO_2. A higher surfactant dipole strength introduces more n_{dope}, n_{imp}, and n^*, such that transport characteristics change more strongly. Moreover, in order to understand the effects of surfactant adsorbates on both sides of graphene, we fabricated suspended devices such that the surfactants can have access to the graphene–dielectric interface. We found that the surfactants also create additional traps (n_{trap}), which capture carriers at high gate voltage, such that strong hysteresis is displayed. The proposed method enables us to eliminate hysteresis to a very high degree and further control it for the first time. These findings facilitate understanding the response of carrier transport to dipole adsorbates and developing novel graphene devices for biosensing and nonvolatile memory applications.

AUTHOR INFORMATION

Corresponding Author

*Email: strano@mit.edu.

Notes

The authors declare no competing financial interest.

ACKNOWLEDGMENTS

C.J.S. is grateful for partial financial support from the Chyn Duog Shiah Memorial Fellowship. D.B. is grateful for the financial support from the DuPont/MIT Alliance. M.S.S. acknowledges funding from the 2009 U.S. Office of Naval Research Multi University Research Initiative (MURI) on Graphene Advanced Terahertz Engineering (GATE) at MIT, Harvard and Boston University. M.S.S. is also grateful for a 2008 Young Investigator Program Award (YIP) from the U.S. Office of Naval Research.

REFERENCES

(1) Geim, A. K.; Novoselov, K. S. The rise of graphene. *Nat. Mater.* **2007**, *6* (3), 183–191.

(2) Ohta, T.; Bostwick, A.; Seyller, T.; Horn, K.; Rotenberg, E. Controlling the electronic structure of bilayer graphene. *Science* **2006**, *313* (5789), 951–954.

(3) Zhang, Y. B.; Tang, T. T.; Girit, C.; Hao, Z.; Martin, M. C.; Zettl, A.; Crommie, M. F.; Shen, Y. R.; Wang, F. Direct observation of a widely tunable bandgap in bilayer graphene. *Nature* **2009**, *459* (7248), 820–823.

(4) Craciun, M. F.; Russo, S.; Yamamoto, M.; Oostinga, J. B.; Morpurgo, A. F.; Thrucha, S. Trilayer graphene is a semimetal with a gate-tunable band overlap. *Nat. Nanotechnol.* **2009**, *4* (6), 383–388.

(5) Zhou, S. Y.; Gweon, G. H.; Fedorov, A. V.; First, P. N.; De Heer, W. A.; Lee, D. H.; Guinea, F.; Neto, A. H. C.; Lanzara, A. Substrate-induced bandgap opening in epitaxial graphene. *Nat. Mater.* **2007**, *6* (11), 916−916.
(6) Novoselov, K. S.; Jiang, D.; Schedin, F.; Booth, T. J.; Khotkevich, V. V.; Morozov, S. V.; Geim, A. K. Two-dimensional atomic crystals. *Proc. Natl. Acad. Sci. U.S.A.* **2005**, *102* (30), 10451−10453.
(7) Sutter, P. W.; Flege, J. I.; Sutter, E. A. Epitaxial graphene on ruthenium. *Nat. Mater.* **2008**, *7* (5), 406−411.
(8) Reina, A.; Jia, X. T.; Ho, J.; Nezich, D.; Son, H. B.; Bulovic, V.; Dresselhaus, M. S.; Kong, J. Large Area, Few-Layer Graphene Films on Arbitrary Substrates by Chemical Vapor Deposition. *Nano Lett.* **2009**, *9* (1), 30−35.
(9) Lee, S.; Lee, K.; Zhong, Z. H. Wafer Scale Homogeneous Bilayer Graphene Films by Chemical Vapor Deposition. *Nano Lett.* **2010**, *10* (11), 4702−4707.
(10) Castro Neto, A. H.; Guinea, F.; Peres, N. M. R.; Novoselov, K. S.; Geim, A. K. The electronic properties of graphene. *Rev. Mod. Phys.* **2009**, *81* (1), 109−162.
(11) dos Santos, J. M. B. L.; Peres, N. M. R.; Castro, A. H. Graphene bilayer with a twist: Electronic structure. *Phys. Rev. Lett.* **2007**, *99* (25), 256802.
(12) Hernandez, Y.; Nicolosi, V.; Lotya, M.; Blighe, F. M.; Sun, Z. Y.; De, S.; McGovern, I. T.; Holland, B.; Byrne, M.; Gun'ko, Y. K.; Boland, J. J.; Niraj, P.; Duesberg, G.; Krishnamurthy, S.; Goodhue, R.; Hutchison, J.; Scardaci, V.; Ferrari, A. C.; Coleman, J. N. High-yield production of graphene by liquid-phase exfoliation of graphite. *Nat. Nanotechnol.* **2008**, *3* (9), 563−568.
(13) Smith, R. J.; Lotya, M.; Coleman, J. N. The importance of repulsive potential barriers for the dispersion of graphene using surfactants. *New J. Phys.* **2010**, *12*, 125008.
(14) Shih, C. J.; Lin, S. C.; Strano, M. S.; Blankschtein, D. Understanding the Stabilization of Liquid-Phase-Exfoliated Graphene in Polar Solvents: Molecular Dynamics Simulations and Kinetic Theory of Colloid Aggregation. *J. Am. Chem. Soc.* **2010**, *132* (41), 14638−14648.
(15) Coleman, J. N. Liquid-Phase Exfoliation of Nanotubes and Graphene. *Adv. Funct. Mater.* **2009**, *19* (23), 3680−3695.
(16) Park, S.; Ruoff, R. S. Chemical methods for the production of graphenes. *Nat. Nanotechnol.* **2009**, *4* (4), 217−224.
(17) Shih, C. J.; Vijayaraghavan, A.; Krishnan, R.; Sharma, R.; Han, J. H.; Ham, M. H.; Jin, Z.; Lin, S. C.; Paulus, G. L. C.; Reuel, N. F.; Wang, Q. H.; Blankschtein, D.; Strano, M. S. Bi- and trilayer graphene solutions. *Nat. Nanotechnol.* **2011**, *6* (7), 439−445.
(18) Martin, J.; Akerman, N.; Ulbricht, G.; Lohmann, T.; Smet, J. H.; Von Klitzing, K.; Yacoby, A. Observation of electron-hole puddles in graphene using a scanning single-electron transistor. *Nat. Phys.* **2008**, *4* (2), 144−148.
(19) Adam, S.; Hwang, E. H.; Galitski, V. M.; Das Sarma, S. A self-consistent theory for graphene transport. *Proc. Natl. Acad. Sci. U.S.A.* **2007**, *104* (47), 18392−18397.
(20) Sabri, S. S.; Levesque, P. L.; Aguirre, C. M.; Guillemette, J.; Martel, R.; Szkopek, T. Graphene field effect transistors with parylene gate dielectric. *Appl. Phys. Lett.* **2009**, *95* (24), 242104.
(21) Lafkioti, M.; Krauss, B.; Lohmann, T.; Zschieschang, U.; Klauk, H.; von Klitzing, K.; Smet, J. H. Graphene on a Hydrophobic Substrate: Doping Reduction and Hysteresis Suppression under Ambient Conditions. *Nano Lett.* **2010**, *10* (4), 1149−1153.
(22) Liu, Z. H.; Bol, A. A.; Haensch, W. Large-Scale Graphene Transistors with Enhanced Performance and Reliability Based on Interface Engineering by Phenylsilane Self-Assembled Monolayers. *Nano Lett.* **2011**, *11* (2), 523−528.
(23) Wang, X. M.; Xu, J. B.; Wang, C. L.; Du, J.; Xie, W. G. High-Performance Graphene Devices on SiO(2)/Si Substrate Modified by Highly Ordered Self-Assembled Monolayers. *Adv. Mater.* **2011**, *23* (21), 2464−2468.
(24) Dean, C. R.; Young, A. F.; Meric, I.; Lee, C.; Wang, L.; Sorgenfrei, S.; Watanabe, K.; Taniguchi, T.; Kim, P.; Shepard, K. L.; Hone, J. Boron nitride substrates for high-quality graphene electronics. *Nat. Nanotechnol.* **2010**, *5* (10), 722−726.
(25) Bolotin, K. I.; Sikes, K. J.; Jiang, Z.; Klima, M.; Fudenberg, G.; Hone, J.; Kim, P.; Stormer, H. L. Ultrahigh electron mobility in suspended graphene. *Solid State Commun.* **2008**, *146* (9−10), 351−355.
(26) Novoselov, K. S.; Schedin, F.; Geim, A. K.; Morozov, S. V.; Hill, E. W.; Blake, P.; Katsnelson, M. I. Detection of individual gas molecules adsorbed on graphene. *Nat. Mater.* **2007**, *6* (9), 652−655.
(27) Dong, X. C.; Fu, D. L.; Fang, W. J.; Shi, Y. M.; Chen, P.; Li, L. J. Doping Single-Layer Graphene with Aromatic Molecules. *Small* **2009**, *5* (12), 1422−1426.
(28) Farmer, D. B.; Golizadeh-Mojarad, R.; Perebeinos, V.; Lin, Y. M.; Tulevski, G. S.; Tsang, J. C.; Avouris, P. Chemical Doping and Electron-Hole Conduction Asymmetry in Graphene Devices. *Nano Lett.* **2009**, *9* (1), 388−392.
(29) Giovannetti, G.; Khomyakov, P. A.; Brocks, G.; Karpan, V. M.; van den Brink, J.; Kelly, P. J. Doping graphene with metal contacts. *Phys. Rev. Lett.* **2008**, *101* (2), 026803.
(30) Szafranek, B. N.; Schall, D.; Otto, M.; Neumaier, D.; Kurz, H. High On/Off Ratios in Bilayer Graphene Field Effect Transistors Realized by Surface Dopants. *Nano Lett.* **2011**, *11* (7), 2640−2643.
(31) Flynn, G. W.; Ryu, S.; Liu, L.; Berciaud, S.; Yu, Y. J.; Liu, H. T.; Kim, P.; Brus, L. E. Atmospheric Oxygen Binding and Hole Doping in Deformed Graphene on a SiO(2) Substrate. *Nano Lett.* **2010**, *10* (12), 4944−4951.
(32) Levesque, P. L.; Sabri, S. S.; Aguirre, C. M.; Guillemette, J.; Siaj, M.; Desjardins, P.; Szkopek, T.; Martel, R. Probing Charge Transfer at Surfaces Using Graphene Transistors. *Nano Lett.* **2011**, *11* (1), 132−137.
(33) Chen, W.; Chen, S.; Qi, D. C.; Gao, X. Y.; Wee, A. T. S. Surface transfer p-type doping of epitaxial graphene. *J. Am. Chem. Soc.* **2007**, *129* (34), 10418−10422.
(34) Ang, P. K.; Chen, W.; Wee, A. T. S.; Loh, K. P. Solution-Gated Epitaxial Graphene as pH Sensor. *J. Am. Chem. Soc.* **2008**, *130* (44), 14392−14393.
(35) Ohno, Y.; Maehashi, K.; Yamashiro, Y.; Matsumoto, K. Electrolyte-Gated Graphene Field-Effect Transistors for Detecting pH Protein Adsorption. *Nano Lett.* **2009**, *9* (9), 3318−3322.
(36) Wang, H. M.; Wu, Y. H.; Cong, C. X.; Shang, J. Z.; Yu, T. Hysteresis of Electronic Transport in Graphene Transistors. *ACS Nano* **2010**, *4* (12), 7221−7228.
(37) Ando, T.; Fowler, A. B.; Stern, F. Electronic-Properties of Two-Dimensional Systems. *Rev. Mod. Phys.* **1982**, *54* (2), 437−672.
(38) Lotya, M.; Hernandez, Y.; King, P. J.; Smith, R. J.; Nicolosi, V.; Karlsson, L. S.; Blighe, F. M.; De, S.; Wang, Z. M.; McGovern, I. T.; Duesberg, G. S.; Coleman, J. N. Liquid Phase Production of Graphene by Exfoliation of Graphite in Surfactant/Water Solutions. *J. Am. Chem. Soc.* **2009**, *131* (10), 3611−3620.
(39) Green, A. A.; Hersam, M. C. Solution Phase Production of Graphene with Controlled Thickness via Density Differentiation. *Nano Lett.* **2009**, *9* (12), 4031−4036.
(40) Chen, F.; Xia, J. L.; Ferry, D. K.; Tao, N. J. Dielectric Screening Enhanced Performance in Graphene FET. *Nano Lett.* **2009**, *9* (7), 2571−2574.
(41) Feldman, B. E.; Martin, J.; Yacoby, A. Broken-symmetry states and divergent resistance in suspended bilayer graphene. *Nat. Phys.* **2009**, *5* (12), 889−893.
(42) Das, A.; Pisana, S.; Chakraborty, B.; Piscanec, S.; Saha, S. K.; Waghmare, U. V.; Novoselov, K. S.; Krishnamurthy, H. R.; Geim, A. K.; Ferrari, A. C.; Sood, A. K. Monitoring dopants by Raman scattering in an electrochemically top-gated graphene transistor. *Nat. Nanotechnol.* **2008**, *3* (4), 210−215.
(43) Berciaud, S.; Ryu, S.; Brus, L. E.; Heinz, T. F. Probing the Intrinsic Properties of Exfoliated Graphene: Raman Spectroscopy of Free-Standing Monolayers. *Nano Lett.* **2009**, *9* (1), 346−352.
(44) Das, A.; Chakraborty, B.; Piscanec, S.; Pisana, S.; Sood, A. K.; Ferrari, A. C. Phonon renormalization in doped bilayer graphene. *Phys. Rev. B* **2009**, *79* (15), 155417.